


# Long-wavelength InAs/InAlGaAs quantum dot microdisk lasers on InP (001) substrate F

Cite as: Appl. Phys. Lett. **122**, 111108 (2023); <https://doi.org/10.1063/5.0142391>

Submitted: 13 January 2023 • Accepted: 27 February 2023 • Published Online: 15 March 2023

 Hui Jia,  Xuezhe Yu,  Taojie Zhou, et al.

## COLLECTIONS

 This paper was selected as Featured



View Online



Export Citation



CrossMark

## ARTICLES YOU MAY BE INTERESTED IN

[Low-threshold visible InP quantum dot and InGaP quantum well lasers grown by molecular beam epitaxy](#)

Journal of Applied Physics **133**, 103101 (2023); <https://doi.org/10.1063/5.0136621>

[Linearly polarized light emission from GaN micro-LEDs for 3D display](#)

Applied Physics Letters **122**, 111107 (2023); <https://doi.org/10.1063/5.0137993>

[Efficient magnetization reversal by self-generated spin-orbit torque in magnetic bulk Rashba materials](#)

Applied Physics Letters **122**, 112405 (2023); <https://doi.org/10.1063/5.0134755>



Time to get excited.  
Lock-in Amplifiers – from DC to 8.5 GHz

[Find out more](#)

 Zurich Instruments

# Long-wavelength InAs/InAlGaAs quantum dot microdisk lasers on InP (001) substrate

Cite as: Appl. Phys. Lett. **122**, 111108 (2023); doi: [10.1063/5.0142391](https://doi.org/10.1063/5.0142391)

Submitted: 13 January 2023 · Accepted: 27 February 2023 ·

Published Online: 15 March 2023










View Online



Export Citation



CrossMark

Hui Jia,<sup>1</sup>  Xuezhe Yu,<sup>1</sup>  Taojie Zhou,<sup>1,2,a)</sup>  Calum Dear,<sup>1</sup>  Jiaping Yuan,<sup>1</sup>  Mingchu Tang,<sup>1</sup>  Zhao Yan,<sup>3</sup>  Bogdan-Petrin Ratiu,<sup>3</sup>  Qiang Li,<sup>3</sup>  Alwyn Seeds,<sup>1</sup>  Huiyun Liu,<sup>1</sup>  and Siming Chen<sup>1,a)</sup> 

## AFFILIATIONS

<sup>1</sup>Electronic and Electrical Engineering, University College London, Torrington Place, London WC1E 7JE, United Kingdom

<sup>2</sup>School of Microelectronics, South China University of Technology, Guangzhou 510641, China

<sup>3</sup>School of Physics and Astronomy, Cardiff University, Cardiff CF24 3AA, United Kingdom

<sup>a)</sup>Authors to whom correspondence should be addressed: [taojiezhou@scut.edu.cn](mailto:taojiezhou@scut.edu.cn) and [siming.chen@ucl.ac.uk](mailto:siming.chen@ucl.ac.uk)

## ABSTRACT

In this Letter, we present long-wavelength microdisk lasers based on five stacks of self-assembled InAs/InAlGaAs quantum dots as the active medium, which were grown on InP (001) substrate by solid-source molecular beam epitaxy. The 8.4- $\mu\text{m}$ -diameter quantum dot microdisk laser is operated at room temperature under pulsed optically pumping conditions. Multi-wavelength lasing emissions at  $\sim 1.6\ \mu\text{m}$  were achieved with a low lasing threshold of  $30\ \mu\text{W}$  and a quality factor of  $\sim 1336$ . The lasing behavior was verified by the “S” shape  $L$ - $L$  curve, linewidth narrowing effect, and strong speckle patterns of the collected near field intensity profile. The demonstrated long-wavelength lasers with low threshold and ultracompact footprint can find potential applications in integrated gas detection and highly localized label-free biological and biochemical sensing.

Published under an exclusive license by AIP Publishing. <https://doi.org/10.1063/5.0142391>

Self-assembled semiconductor quantum dot (QD) lasers have attracted considerable attention and present superior performance compared to conventional quantum-well (QW) or bulk counterparts, owing to their zero-dimensionality properties.<sup>1</sup> In recent years, semiconductor QD lasers with ultralow lasing threshold,<sup>2–5</sup> high temperature stability,<sup>6</sup> and low-chirp operation<sup>7</sup> have been reported. However, these remarkable achievements have mainly been demonstrated based on InAs/GaAs QDs, where the emitting wavelength is limited up to around  $1.3\ \mu\text{m}$ .<sup>8–10</sup> InAs QDs grown on an InP substrate have a wider range of applications as they can produce a wider and longer wavelength range from  $1.4$  to  $2.5\ \mu\text{m}$  (Refs. [11–15](#)) for use in fiber optic telecommunication systems and sensing.<sup>16,17</sup>

On the other hand, the miniaturization of semiconductor lasers offers advanced approaches toward high density photonic integration.<sup>18</sup> Among various types of small lasers, the microdisk laser has received intense research interest due to its planar microcavity structure and a simple fabrication scheme,<sup>4,19</sup> paving the way to highly compact integrated light sources and allowing easy integration with a passive bus waveguide component.<sup>20,21</sup> High quality factor (Q-factor) whispering gallery modes (WGMs) are tightly confined in the microdisk cavities that result from total internal reflection of traveling waves. Notably, microdisk lasers hold distinct advantages of both low power

consumption and ultracompact device footprint. However, low threshold InAs QD microdisk lasers with emitting wavelength longer than  $1.6\ \mu\text{m}$  are rarely investigated, which have promising prospects in integrated gas detection<sup>22</sup> and highly localized label-free biological and biochemical sensing.<sup>23–26</sup> The main challenge is to grow high quality of InAs QDs on the InP substrate due to the low lattice mismatch and the As-P exchange at the growth interface.<sup>27,28</sup>

Here, we report long-wavelength InAs/InAlGaAs QD microdisk lasers on the InP substrate grown by solid-source molecular beam epitaxy (MBE), combining the important advantages of both small footprint and the discrete atomic-like characteristic of QD electronic states. The InAs/InAlGaAs QD microdisk lasers were optically pumped at room temperature to give multi-wavelength emission around  $1.6\ \mu\text{m}$  and a low lasing threshold of approximately  $30\ \mu\text{W}$ .

The structure under investigation was grown on an n-type InP (001) substrate by MBE equipped with a valved arsenic cracker source and a valved phosphorus cracker. Prior to the epitaxial growth, the substrate was first degassed at  $400\ ^\circ\text{C}$  for 1 h in the preparation chamber, then transferred to the growth chamber and heated to  $500\ ^\circ\text{C}$  under  $\text{As}_2$  overpressure for 1 min to remove surface oxides. The epitaxial structure consists of  $10\ \text{nm}\ \text{In}_{0.532}\text{Ga}_{0.468}\text{As}$  and  $40\ \text{nm}\ \text{In}_{0.524}\text{Al}_{0.476}\text{As}$  lattice-matched to InP as the cladding layers and five

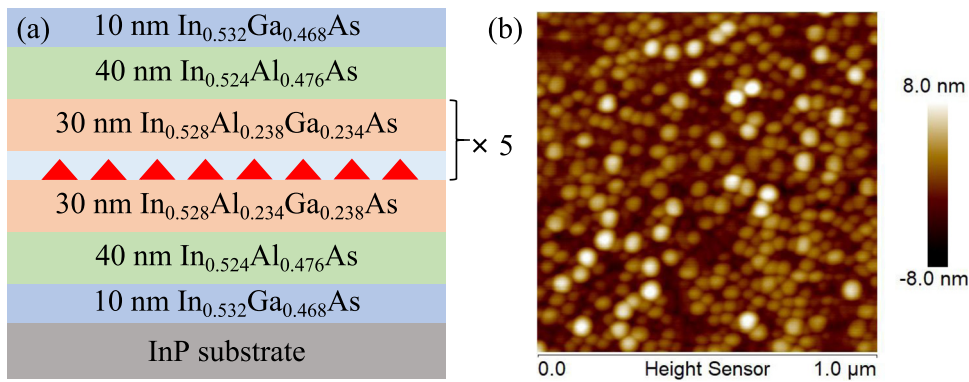


**FIG. 1.** (a) Schematic illustration of the epitaxial structure of InAs/InAlGaAs QD microdisk lasers. (b) An AFM image of uncapped InAs/InAlGaAs QDs.

repeats of nominal 5.5 monolayers (ML) thick InAs QDs separated by 30 nm  $\text{In}_{0.528}\text{Al}_{0.234}\text{Ga}_{0.238}\text{As}$  barrier layers. The growth temperatures for InGaAs and InAlAs were 500 and 510 °C, respectively. The InAs QDs were grown in an  $\text{As}_2$  mode at 485 °C with a growth rate of 0.42 ML/s. A growth interruption of 10 s was applied to facilitate the QDs formation and enhance the QDs uniformity. After the growth of each QD layer, 4 nm  $\text{In}_{0.528}\text{Al}_{0.234}\text{Ga}_{0.238}\text{As}$  was deposited at the same substrate temperature to partially cover the QDs. Then the substrate temperature was rapidly elevated to 540 °C and held for 1 min to evaporate the exposed InAs and achieve high QD uniformity. Subsequently, the remaining 26 nm  $\text{In}_{0.528}\text{Al}_{0.234}\text{Ga}_{0.238}\text{As}$  layer was grown at 500 °C. The top InGaAs cladding layer was deposited as an InAlAs cladding layer is prone to oxidation. Figure 1(a) shows the schematic diagram of an epitaxial layer structure with five stacks of InAs QDs as gain materials, where the thickness of the entire active layer is around 280 nm. An atomic force microscope (AFM) image of uncapped InAs/InAlGaAs QDs is presented in Fig. 1(b), indicating a density of  $\sim 4.4 \times 10^{10} \text{ cm}^{-2}$ .

To fabricate the InAs/InAlGaAs QD microdisk lasers, first, a layer of silicon nitride with a thickness of around 150 nm was deposited as the hard mask on the epitaxial wafer by plasma enhanced chemical vapor deposition. A layer of 300 nm PMMA A4 electron beam resist was then spin coated on the surface of the hard mask. Subsequently, the microdisk pattern in PMMA was defined using electron beam lithography and transferred into the silicon nitride layer using reactive ion etching (RIE) with a mixture etching gas of  $\text{CHF}_3$  and  $\text{O}_2$ . Afterwards, the pattern was further transferred into the active region and the InP sacrificial layer by using inductively coupled plasma RIE (ICP-RIE) based on a mixture of  $\text{BCl}_3$  and  $\text{H}_2$ . Finally, wet etching was used to remove the residual hard mask and form the supporting pedestals for suspending microdisk cavities. Figure 2(a) presents a tilted SEM image of the fabricated InAs/InAlGaAs QD microdisk laser array. The inset in Fig. 2(a) displays a top view SEM image of a microdisk laser. Light is strongly confined in-plane by successive total internal reflections at the smooth periphery to form the high Q-factor WGMs with small mode volume.<sup>29</sup> Figure 2(b) shows a tilted SEM image of a typical fabricated microdisk laser, showing the smooth etched sidewall and a small mechanically supporting pedestal. The distance between the supporting pedestal and the microdisk boundary is more than  $3 \mu\text{m}$ , avoiding the loss of light coupling of WGMs from the microdisk cavity into the pedestal.

The fabricated InAs/InAlGaAs QD microdisk lasers were optically pumped at room temperature with a micro-PL measurement system in a surface normal pumping configuration by using a 632 nm red emission laser (100 ps pulses separated by 100 ns period) as the pumping source. The pumping beam was focused on the microdisk cavity with a spot size of  $\sim 12 \mu\text{m}$  in diameter through a  $\times 50$  objective lens. The emission spectra of the microdisk lasers were collected from the top by using the same objective lens and further analyzed by a monochromator with an InGaAs detector. A long-wavelength-pass filter was used to block the excitation light from reaching the InGaAs detector. The near-field intensity profiles of the microdisk lasers were collected by the same InGaAs detector.

Figure 3(a) presents the measured lasing spectra of a microdisk laser with a diameter around  $8.4 \mu\text{m}$ . The inset in Fig. 3(a) displays the

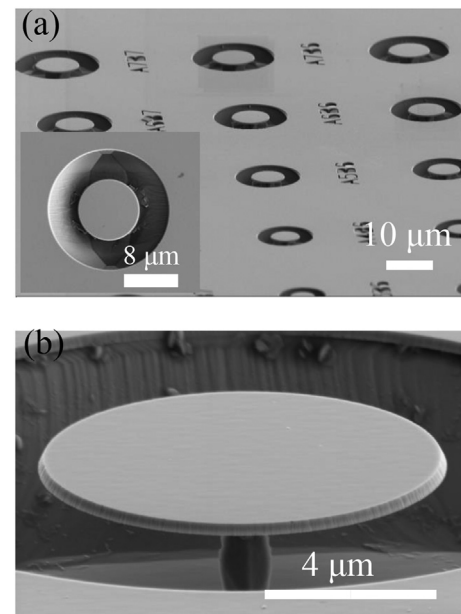


**FIG. 2.** (a) A tilted SEM image of the fabricated InAs/InAlGaAs QD microdisk laser array. The inset shows a top view SEM image of the fabricated microdisk laser. (b) A tilted SEM image of the fabricated microdisk laser.

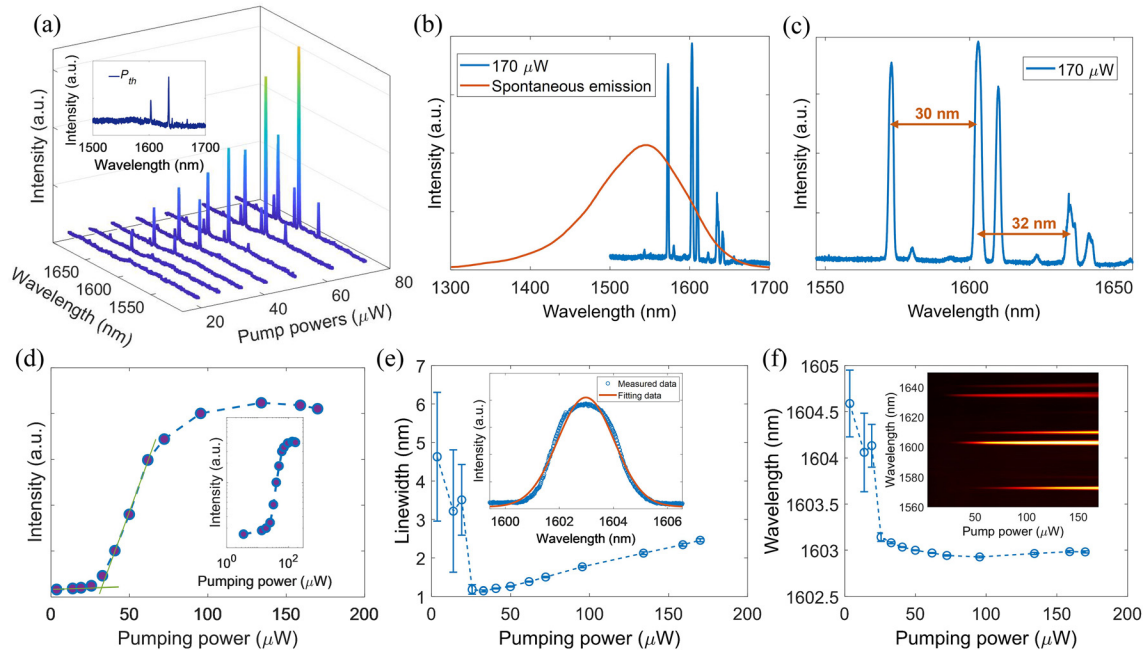


**FIG. 3.** (a) Collected lasing spectra under various pumping powers. The inset in (a) displays a measured lasing spectrum near the lasing threshold. (b) The collected lasing spectrum (blue) under pumping power  $170 \mu\text{W}$  (above the lasing threshold) of a microdisk laser and the spontaneous emission spectrum (orange) of the unpattern region. (c) An enlarged laser spectrum of the microdisk laser, indicating that an experimental FSR is around  $30 \text{ nm}$ . The lasing peak at  $1603 \text{ nm}$  was identified as  $\text{TE}_{1,41}$  from simulation. (d) The  $L$ - $L$  curve in the linear scale and logarithmic scale (shown in the inset). (e) Linewidths of the lasing peak under various pumping powers. The inset shows the Gaussian curve fitting of the experimental data. (f) Lasing wavelengths under various pumping powers. The inset in (b) presents the collected spectra under various pumping powers.

lasing spectra collected near the lasing threshold of the lasing peak at  $1603 \text{ nm}$ , showing that the resonant peaks grow up from the spontaneous emission background. The spontaneous emission background is strongly compressed after reaching the lasing threshold, as shown in Fig. 3(b). The microdisk lasers can support multi high  $Q$ -factor first-order WGMs, resulting in mode competition and multimode lasing emission. As shown in Fig. 3(c), the lasing spectrum exhibits multimode operation under elevated pumping powers. The free spectral range (FSR) of the microdisk laser with diameter  $\sim 8.4 \mu\text{m}$  can be estimated by using the following equation:  $\text{FSR} = \frac{c^2}{\pi D n_{\text{eff}}} \sim \frac{(1603 \text{ nm})^2}{\pi * (8.3 \mu\text{m}) * 2.9} = 36.6 \text{ nm}$ , supposing an effective refractive index  $n_{\text{eff}} = 2.9$ . The calculated FSR is consistent with the experimental value, as shown in Fig. 3(c).

The lasing threshold is estimated from the light in-light out ( $L$ - $L$ ) curve. A low lasing threshold of approximately  $30 \mu\text{W}$  is extracted from  $L$ - $L$  curve of the lasing peak at  $1603 \text{ nm}$ , as shown in Fig. 3(d). A clear kink in the  $L$ - $L$  curve can be observed with an obvious “S” shape in the logarithmic scale shown in the inset in Fig. 3(d), implying a transition from spontaneous emission to stimulated emission. At elevated pumping powers (above  $\sim 70 \mu\text{W}$ ), the collected intensity of the InAs/InAlGaAs QD microdisk laser begins to saturate, mostly because of gain saturation. The lasing operation is further verified by the linewidth narrowing effect, as shown in Fig. 3(e). A clear linewidth narrowing effect can be observed around the lasing threshold with a narrow linewidth of  $\sim 1.2 \text{ nm}$  above the lasing threshold.

The increase in the linewidth above threshold is mainly attributed to the temporal shift in the lasing frequency.<sup>30</sup> The linewidths of the lasing peaks are obtained by using Gaussian curve fitting of the experimental data as shown in the inset in Fig. 3(e). The cavity  $Q$ -factor of the fabricated InAs/InAlGaAs QD microdisk laser is estimated from the linewidth just below the lasing threshold, where the optical loss by the absorption of the QDs is extremely small. The linewidth measured at just below the threshold corresponds to a value of  $Q$ -factor  $\sim 1336$ . The  $Q$ -factor can be further increased by optimizing the fabrication processes to achieve smoother sidewalls of the microdisk cavities, and the threshold can be further decreased by using the surface passivation method to suppress the non-radiative Auger recombination.<sup>31</sup> The lasing wavelengths under various pumping powers are depicted in Fig. 3(f). A rapid blue shift of the lasing wavelength can be observed near the lasing threshold, which is mainly contributed to the carrier plasma effects.<sup>32</sup> The inset in Fig. 3(f) presents the spectra collected under various pumping powers. There is no significant red shift of lasing peaks with increasing pumping powers after reaching the threshold, indicating that there is no remarkable heat accumulation due to thermal effect under an optical pulse pumping method. This is because short pulses ( $100 \text{ ps}$  width separated by  $100 \text{ ns}$  period) are used to excite the lasing emission during the optical pumping process, thus allowing sufficient time for heat dissipation. To verify the lasing mode, near field intensity profiles are captured by using an InGaAs camera, as shown in Fig. 4. Before reaching the lasing threshold, the emission of the microdisk cavity is predominated by spontaneous

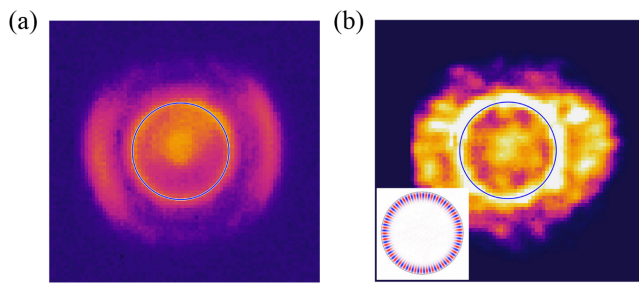


**FIG. 4.** (a) and (b) The collected near field intensity profile images below and above the lasing threshold, respectively. The blue circle indicates the boundary of the microdisk lasers. The inset in (b) shows the calculated magnetic field ( $H_z$ ) profile of  $TE_{1,41}$  WGM.

emission with a relatively uniform intensity distribution. After reaching the lasing threshold, stimulated emission dominates and forms tightly confined WGMs along the circular boundary. Light distributes at the circular boundary with pronounced speckle patterns, resulting from the high degree of coherent emission as shown in Fig. 4(b).

In conclusion, we reported room temperature optically pumped long-wavelength microdisk lasers with five stacks of InAs/InAlGaAs QD as gain materials grown by MBE. Lasing emission at  $\sim 1.6 \mu\text{m}$  and a low lasing threshold of  $\sim 30 \mu\text{W}$  were observed in an  $8.4\text{-}\mu\text{m}$ -diameter InAs/InAlGaAs QD microdisk laser. The demonstrated long-wavelength microdisk laser with low threshold and small footprint provides a promising route toward integrated gas detection and highly localized label-free biological and biochemical sensing.

This work was supported by the UK Engineering and Physical Sciences Research Council (Nos. EP/V029606/1, EP/W002302/1, EP/V029681/1, EP/T01394X/1, and EP/P006973/1), the National Epitaxy Facility, Royal Academy of Engineering (No. RF201617/16/28), and the European Project H2020-ICT-PICTURE (No. 780930).

## AUTHOR DECLARATIONS

### Conflict of Interest

The authors have no conflicts to disclose.

### Author Contributions

Hui Jia, Xuezhe Yu, and Taojie Zhou contributed equally to this work.

**Hui Jia:** Data curation (lead); Investigation (equal); Writing – original draft (equal); Writing – review & editing (equal). **Alwyn Seeds:** Writing – review & editing (equal). **Huiyun Liu:** Funding acquisition (equal); Supervision (equal); Writing – review & editing (equal). **Siming Chen:** Funding acquisition (equal); Supervision (lead); Writing – review & editing (equal). **Xuezhe Yu:** Investigation (equal); Writing – review & editing (equal). **Taojie Zhou:** Data curation (equal); Investigation (equal); Supervision (equal); Writing – original draft (lead); Writing – review & editing (equal). **Calum Dear:** Writing – review & editing (equal). **Jiajing Yuan:** Writing – review & editing (equal). **Mingchu Tang:** Writing – review & editing (equal). **Zhao Yan:** Data curation (equal). **Bogdan-Petrin Ratiu:** Data curation (equal). **Qiang Li:** Data curation (equal); Writing – review & editing (equal).

## DATA AVAILABILITY

The data that support the findings of this study are available from the corresponding authors upon reasonable request.

## REFERENCES

- F. P. García de Arquer, D. V. Talapin, V. I. Klimov, Y. Arakawa, M. Bayer, and E. H. Sargent, *Science* **373**(6555), eaaz8541 (2021).
- T. Zhou, M. Tang, G. Xiang, B. Xiang, S. Hark, M. Martin, T. Baron, S. Pan, J.-S. Park, Z. Liu, S. Chen, Z. Zhang, and H. Liu, *Nat. Commun.* **11**(1), 977 (2020).
- T. Zhou, J. Ma, M. Tang, H. Li, M. Martin, T. Baron, H. Liu, S. Chen, X. Sun, and Z. Zhang, *ACS Photonics* **9**(12), 3824–3830 (2022).
- T. Zhou, M. Tang, G. Xiang, X. Fang, X. Liu, B. Xiang, S. Hark, M. Martin, M.-L. Touraton, T. Baron, Y. Lu, S. Chen, H. Liu, and Z. Zhang, *Optica* **6**(4), 430–435 (2019).
- T. Zhou, M. Tang, H. Li, Z. Zhang, Y. Cui, J.-S. Park, M. Martin, T. Baron, S. Chen, and H. Liu, *IEEE J. Sel. Top. Quantum Electron.* **28**(3), 1–6 (2021).
- L. V. Asryan and S. Luryi, *Solid-State Electron.* **47**(2), 205–212 (2003).
- H. Saito, K. Nishi, A. Kamei, and S. Sugou, *IEEE Photonics Technol. Lett.* **12**(10), 1298–1300 (2000).
- H. Liu, T. Wang, Q. Jiang, R. Hogg, F. Tutu, F. Pozzi, and A. Seeds, *Nat. Photonics* **5**(7), 416–419 (2011).
- A. Zhukov, A. Kovsh, N. Maleev, S. Mikhlin, V. Ustinov, A. Tsatsul'nikov, M. Maximov, B. Volovik, D. Bedarev, and Y. M. Shernyakov, *Appl. Phys. Lett.* **75**(13), 1926–1928 (1999).
- J. C. Norman, D. Jung, Z. Zhang, Y. Wan, S. Liu, C. Shang, R. W. Herrick, W. W. Chow, A. C. Gossard, and J. E. Bowers, *IEEE J. Quantum Electron.* **55**(2), 1–11 (2019).
- Y. Qiu, D. Uhl, R. Chacon, and R. Q. Yang, *Appl. Phys. Lett.* **83**(9), 1704–1706 (2003).
- S. Luo, H.-M. Ji, F. Gao, X.-G. Yang, P. Liang, L.-J. Zhao, and T. Yang, *Chin. Phys. Lett.* **30**(6), 068101 (2013).
- S. Fafard, Z. Wasilewski, J. McCaffrey, S. Raymond, and S. Charbonneau, *Appl. Phys. Lett.* **68**(7), 991–993 (1996).
- H. Li, T. Daniels-Race, and Z. Wang, *J. Cryst. Growth* **200**(1–2), 321–325 (1999).
- C. Paranthoen, N. Bertru, O. Dehaese, A. Le Corre, S. Louliche, B. Lambert, and G. Patriarche, *Appl. Phys. Lett.* **78**(12), 1751–1753 (2001).
- S. Zhu, B. Shi, Q. Li, and K. M. Lau, *Appl. Phys. Lett.* **113**(22), 221103 (2018).
- G. Liu, P. J. Poole, Z. Lu, J. Liu, Y. Mao, M. Vachon, and P. Barrios, *Opt. Express* **30**(3), 3205–3214 (2022).
- M. T. Hill and M. C. Gather, *Nat. Photonics* **8**(12), 908–918 (2014).
- T. Zhou, K. W. Ng, X. Sun, and Z. Zhang, *Nanophotonics* **9**(9), 2997–3002 (2020).
- C. S. June, K. Djordjevic, C. S. Jun, and P. D. Dapkus, *IEEE Photonics Technol. Lett.* **15**(10), 1330–1332 (2003).
- J. van Campenhout, P. Rojo-Romeo, P. Regreny, C. Seassal, D. van Thourhout, S. Verstuyft, L. di Cioccio, J.-M. Fedeli, C. Lagahe, and R. Baets, *Opt. Express* **15**(11), 6744–6749 (2007).
- W. Gong, J. Hu, Z. Wang, Y. Wei, Y. Li, T. Zhang, Q. Zhang, T. Liu, Y. Ning, W. Zhang, and K. T. V. Grattan, *Front. Phys.* **10**, 58475 (2022).
- N. Toropov, G. Cabello, M. P. Serrano, R. R. Gutha, M. Rafti, and F. Vollmer, *Light: Sci. Appl.* **10**(1), 42 (2021).
- T. Pan, D. Lu, H. Xin, and B. Li, *Light: Sci. Appl.* **10**(1), 124 (2021).
- A. H. Fikouras, M. Schubert, M. Karl, J. D. Kumar, S. J. Powis, A. Di Falco, and M. C. Gather, *Nat. Commun.* **9**(1), 4817 (2018).
- N. Martino, S. J. J. Kwok, A. C. Liapis, S. Forward, H. Jang, H.-M. Kim, S. J. Wu, J. Wu, P. H. Dannenberg, S.-J. Jang, Y.-H. Lee, and S.-H. Yun, *Nat. Photonics* **13**(10), 720–727 (2019).
- S. Hasan, C. Merckling, M. Pantouvaki, J. Meerschaut, J. Van Campenhout, and W. Vandervorst, *J. Cryst. Growth* **509**, 133–140 (2019).
- R. S. R. Gajjala, E. M. Sala, J. Heffernan, and P. M. Koenraad, *ACS Appl. Nano Mater.* **5**(6), 8070–8079 (2022).
- W. Noh, M. Dupré, A. Ndao, A. Kodigala, and B. Kanté, *ACS Photonics* **6**(2), 389–394 (2019).
- Q. Song, H. Cao, S. Ho, and G. Solomon, *Appl. Phys. Lett.* **94**(6), 061109 (2009).
- K. Kuruma, Y. Ota, M. Kakuda, S. Iwamoto, and Y. Arakawa, *APL Photonics* **5**(4), 046106 (2020).
- M. Fujita, R. Ushigome, and T. Baba, *IEEE Photonics Technol. Lett.* **13**(5), 403–405 (2001).